Measurement of Glass Plate Thickness and Refractive Index using Brewster's Angle and Two-Beam Interference

Natalia Tabja
Department of Physics, University of Toronto
(Dated: April 4, 2025)

We demonstrate two complementary methods to characterize a glass plate: (1) determination of its refractive index via Brewster's angle, and (2) thickness measurement from two-beam interference akin to a double-slit experiment. From the Brewster angle, we obtain an index of refraction $n = 1.45 \pm 0.05$, and from the fringe spacing, we extract a thickness $t = (1.028 \pm 0.020)$ mm. Both values are in excellent agreement with standard references for soda-lime glass.

INTRODUCTION

Index of Refraction

When an electromagnetic wave encounters an interface between two media with refractive indices n_i and n_t, the amplitudes of the reflected (r) and transmitted (t) waves differ depending on the polarization and incidence angle θ_i. According to Fresnel's equations [4], the reflection coefficient for p-polarized light traveling between media with indices of refraction n_i and n_t respectively, can be written as

$$r_p(\theta_i) = \frac{n_t \cos\theta_i - n_i \cos\theta_t}{n_t \cos\theta_i + n_i \cos\theta_t},$$

where θ_t follows Snell's law, $\sin(\theta_t) = (n_i/n_t)\sin(\theta_i)$. The reflected intensity is $R_p = |r_p|^2$. Figure 1 shows the theoretical curves for R_s and R_p as a function of θ_i for $n_t = 1.5$. Note that R_p displays a pronounced dip where p-polarized reflection vanishes.

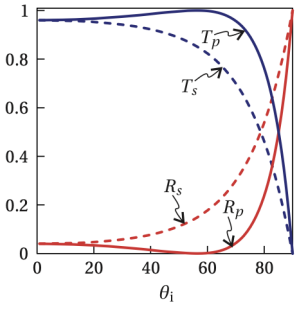

FIG. 1. Theoretical reflectance (R_s, R_p) and transmittance (T_s, T_p) vs. incidence angle θ_i at an air–glass interface ($n_t = 1.5$), from Ref. [4]. Brewster's angle ($\theta_B \approx 56^\circ$) is where R_p goes to zero.

A key consequence is *Brewster's angle* θ_B, at which $R_p(\theta_B) = 0$. Solving for $r_p = 0$ leads directly to

$$\tan(\theta_B) = \frac{n_t}{n_i}. \tag{1}$$

Hence, to determine the refractive index n_t of the glass, one illuminates the sample with p-polarized light, varies θ_i until the reflected intensity R_p reaches its minimum, and records that angle as θ_B. The refractive index is then $n_t = \tan(\theta_B)$, where $n_i = 1.000271800$ for air[3].

Plate Thickness

A second objective is to measure the thickness t of a glass plate. When laser light reflects off both the front and back surfaces of a plane–parallel slab, two partial beams emerge in parallel but are laterally displaced by a distance d. In the far field, these two beams act analogously to slits in a double-slit experiment, producing an interference pattern with fringe spacing

$$\Delta x = \frac{\lambda L}{d}, \tag{2}$$

where λ is the laser wavelength and L is the distance from the sample to the camera.

To relate the beam separation d to the slab thickness t, we consider the internal geometry shown in Fig. 2. A beam entering at angle θ_i refracts to angle θ_t and travels a lateral distance $D/2$ across the slab before reflecting. Simple trigonometry gives

$$\tan(\theta_t) = \frac{D/2}{t} \quad \Rightarrow \quad D = 2t\tan(\theta_t).$$

Projecting this distance back onto the external axis, we find

$$\cos(\theta_i) = \frac{d}{D} \quad \Rightarrow \quad d = D\cos(\theta_i).$$

Substituting for D, and using Snell's Law to find θ_t, we obtain

$$d = 2t\tan(\theta_t)\cos(\theta_i), \quad \theta_t = \sin^{-1}\left(\frac{\sin\theta_i}{n}\right) \tag{3}$$

which, when combined with Eq. (2), yields

$$t = \frac{\lambda\, L}{2\,\Delta x\,\tan(\theta_t)\,\cos(\theta_i)} \tag{4}$$

Once the incidence angle θ_i and the refractive index n (determined via Brewster's angle) are known, measuring the fringe spacing Δx directly allows for a precise measurement of the slab thickness t.

Because the back-reflected beam travels farther inside the slab, it is crucial to focus the laser near the front surface to ensure good overlap of the two reflected beams in the far field. According to geometric optics, the only way to further reduce the beam waist (and thus improve overlap) is to use a shorter focal length lens or expand the input beam [7]. We tested several biconvex lenses with varying focal lengths to optimize fringe visibility and facilitate accurate measurement of t.

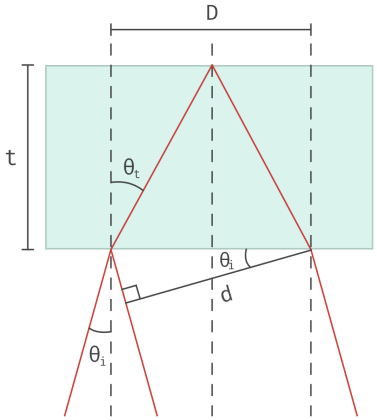

FIG. 2. Schematic of the internal reflection geometry for a plane–parallel slab. The beam at external angle θ_i refracts at angle θ_t, yielding a lateral displacement $d = 2\,t\,\tan(\theta_t)\,\cos(\theta_i)$.

In this report, we implement these two complementary methods on a glass slide. First, we locate the Brewster angle θ_B by monitoring p-polarized reflectance as a function of θ_i. Second, we focus the laser onto the slide at a known incidence angle and record the resulting two-beam interference fringes on a CMOS camera to find t. A HeNe laser at $\lambda = 633\,\text{nm}$ was used throughout. Our results indicate $n = 1.45 \pm 0.05$ and $t = 1.028 \pm 0.020\,\text{mm}$, well within expectations for common soda-lime glass.

METHODS

Brewster Angle Setup and Measurement

A HeNe laser ($\lambda = 633\,\text{nm}$) was directed at the glass slab at varying incidence angles θ_i near the expected Brewster angle $\theta_B \approx 56°$. As shown schematically in Fig. 3, a quarter-wave plate (QWP) was positioned immediately after the laser, oriented at approximately 45° to the horizontal, thereby generating elliptically polarized light. A linear polarizer and photodiode were placed several centimeters beyond the reflected beam to detect p-polarized light selectively.

We recorded the detector voltage at six incidence angles, from 47° to 61°, in order to locate the angle θ_B of minimal reflected power. An ND filter (optical density 0.7) prevented detector saturation, yielding a consistent background of $-1 \pm 2\,\text{mV}$. After subtracting this offset, we performed a quadratic fit to the intensity vs. angle data to approximate the minimum. Despite the exact Fresnel form not being strictly parabolic, the local minimum near Brewster's angle is well-captured by such a fit. Once θ_B was identified, the refractive index followed directly from $n_t = n_i \tan(\theta_B)$, and the known index of refraction for air (n_i).

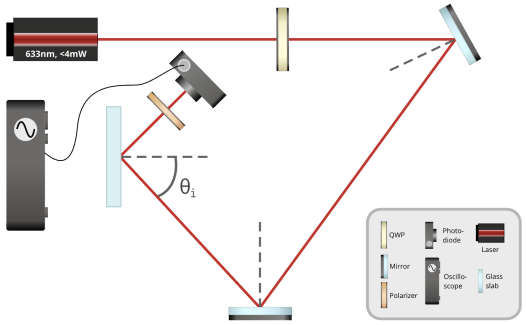

FIG. 3. Schematic of the Brewster angle setup. A HeNe laser passes through a quarter-wave plate and strikes the glass slab at angle θ_i. Reflected light is then filtered by a polarizer and detected by a photodiode connected to an oscilloscope.

Two-Beam Interference for Thickness

To determine the plate thickness t, we recorded the interference fringes produced by overlapping reflections from the front and back surfaces of the glass slide. A biconvex lens was used to focus the HeNe laser ($\lambda = 633\,\text{nm}$) near the front surface of the slab, enhancing beam overlap in the far field.

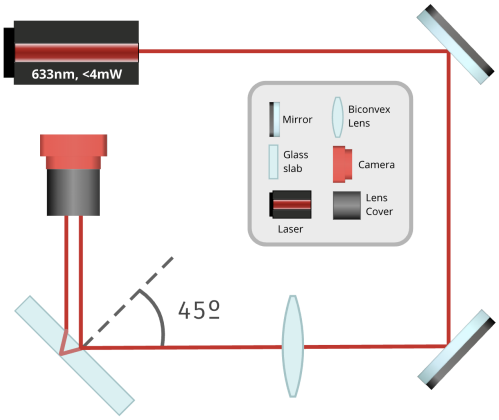

FIG. 4. Experimental setup for the thickness measurement. A biconvex lens focuses the beam at $\theta_i \approx 45°$ onto the glass slab, and a CMOS camera at distance L records the overlapping front/back reflections and resulting interference fringes.

The slab was tilted at an angle $\theta_i \approx 45°$, and the resulting interference pattern was captured by an Allied Vision Alvium 1800 U-500m CMOS camera (5.0 MP, 1/2.5" sensor)[1], placed a distance L downstream.

Consecutive fringe centers were manually selected using a custom program written in Processing [5], a Java-based graphical environment. Processing was chosen over Python due to its built-in image-handling and interactive GUI features, enabling fast and precise fringe identification. A full-field fringe image and a close-up of the fringe selection process are shown in Figs. 5 and 6.

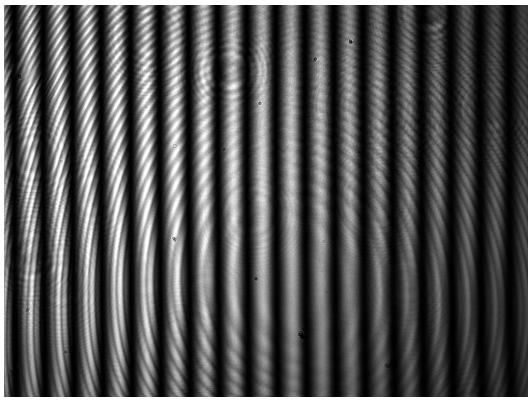

FIG. 5. Full fringe pattern recorded on the CMOS camera, here using a 75 mm focal length lens. Interference arises from front- and back-surface reflections of the glass slab.

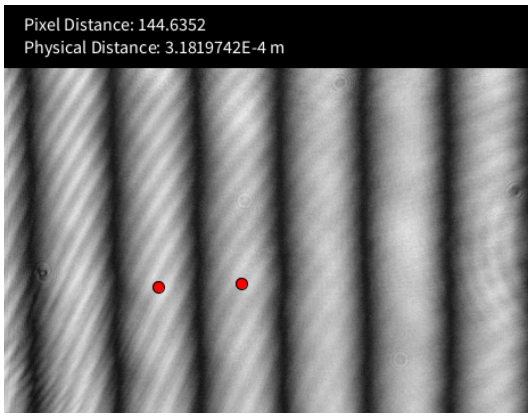

FIG. 6. Close-up of fringe analysis. Fringe centers (red dots) were manually selected in `Processing` to determine the fringe spacing Δx.

From the measured fringe spacing Δx, we determined the lateral displacement d using Eq. (2). We then applied equation (4) to compute t, using the index of refraction obtained from our Brewster angle analysis.

Multiple lenses with focal lengths ranging from 25.4 mm to 100 mm were tested to ensure robust fringe visibility under different beam-convergence angles. The lens-to-slab distance was set to the focal length of the lens in order to maintain the beam waist near the front surface. This maximized the overlap of the two reflected beams in the far field.

RESULTS

Index of Refraction via Brewster's Angle

We measured the reflected intensity at six angles from 47° to 61°, each with an angular uncertainty of ±1°. The photodiode voltage was recorded with a Keysight DSOX1202G oscilloscope [2], carrying ±6.3 mV uncertainty, plus ±2 mV from ND filter fluctuations (added in quadrature). After subtracting a constant −1 mV offset, a quadratic fit located the minimum at $\theta_B = (55.4 \pm 1)°$, see Fig. 7. Despite a $\chi^2_{\text{red}} \approx 27.3$ indicating some systematic deviations, we interpret the fit vertex as the Brewster angle.

This high value of χ^2_{red} is not due to random noise, but rather reflects the fact that a quadratic is only an approximate model for the Fresnel reflectance curve near its minimum. In particular, the measured reflectance outside the dip deviates more strongly from the parabolic fit, contributing disproportionately to the residuals. Additionally, the high χ^2_{red} is partly explained by the fact that our uncertainties in the y-axis (photodiode voltage) are quite small compared to the relatively large uncertainties in the x-axis (angle), which are not accounted for in the standard fit.

Nevertheless, the vertex of the fit clearly identifies the minimum reflectance angle, allowing us to estimate the refractive index as

$$n = n_i \tan(\theta_B) = 1.45 \pm 0.05,$$

which matches typical values for soda-lime glass at $\lambda = 633$ nm [6].

The uncertainty was calculated via standard error propagation:

$$\sigma_n = \left| \frac{dn}{d\theta_B} \right| \sigma_{\theta_B} = \sec^2(\theta_B)\, \sigma_{\theta_B}.$$

Substituting $\theta_B = 55°$ and $\sigma_{\theta_B} = 1° = 0.0175$ rad gives

$$\sigma_n = \sec^2(55°) \cdot 0.0175 \approx 0.054 \approx 0.05.$$

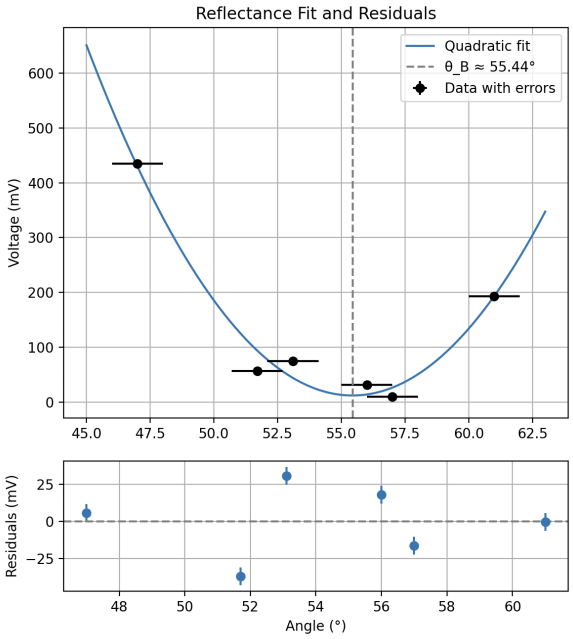

FIG. 7. Measured reflectance (photodiode voltage) vs. angle. A parabolic fit approximates the local minimum near θ_B, yielding $n = 1.45 \pm 0.05$. Bottom: fit residuals show some systematic offset, but the global minimum is clear.

Plate Thickness via Interference

Next, we combined $\theta_i = 45° \pm 1°$ and $n = 1.45 \pm 0.05$ to compute t for each lens configuration. The camera distance was $L = (39.0 \pm 0.5)$ cm. Fringe spacing Δx was extracted from images using a 2.2 µm per-pixel scale [1], with ±2-pixel ($\pm 4.4\,\mu$m) uncertainty. Table I lists the resulting thickness for each focal length, along with a weighted average.

TABLE I. Measured fringe spacing and calculated plate thickness for each lens. Final row shows weighted mean and standard error.

Focal Length (mm)	**Fringe Spacing** (mm)	**Thickness** t (mm)
25.4	0.3266 ± 0.0044	0.957 ± 0.037
35.0	0.3179 ± 0.0044	0.983 ± 0.038
50.0	0.2265 ± 0.0044	1.380 ± 0.055
75.0	0.3179 ± 0.0044	0.983 ± 0.038
100.0	0.3049 ± 0.0044	1.025 ± 0.040
Weighted Mean	—	$\mathbf{1.028 \pm 0.020}$

A weighted mean was used to compute the best estimate of the plate thickness t, recognizing that not all measurements carried equal precision. Although the uncertainty in fringe spacing Δx was held fixed across lenses, the nonlinear dependence of t on Δx caused the propagated uncertainties in t to vary by up to 50%. To account for this, we used inverse-variance weighting: each measurement was weighted by $1/\sigma_t^2$, ensuring that more precise data contributed more strongly to the final average. This statistically grounded approach yields a more accurate and reliable estimate than a simple arithmetic mean.

Thickness values are mostly consistent (0.95-1.03 mm) except for the 50 mm lens, which produced a significantly higher value (1.38 mm). This outlier may reflect beam misalignment, defocusing, or partial saturation in the image. Nevertheless, the weighted average $t = (1.028 \pm 0.020)$ mm is physically reasonable for a standard glass slide, and the small standard error suggests strong reproducibility across different optical configurations.

Discussion

Brewster's Angle Fit. Figure 7 shows the measured reflectance proxy (photodiode voltage) versus incidence angle. Although the best-fit parabola yields a well-defined minimum, the reduced chi-squared ($\chi^2_{\text{red}} \approx 27.3$) is larger than unity. This suggests systematic deviations—likely from minor misalignment, incomplete p-polarization, or residual background fluctuations that vary with angle. In particular, the data near 52° sits below the fitted curve, while angles near 58° exceed it by tens of millivolts. Nonetheless, the global minimum is clear, and the vertex angle $\theta_B = (55.4 \pm 1)°$ is in line with the expected range for soda-lime glass. Using $n = \tan(\theta_B)$ is a well-established procedure for p-polarized reflection at dielectric interfaces, and our final $n = 1.45 \pm 0.05$ is entirely consistent with tabulated values (1.45-1.50). A more refined angular sweep or improved polarization control (e.g., adding an initial half-wave plate) might reduce the systematic scatter, lowering χ^2_{red} closer to unity.

Fringe Pattern and Thickness. For the thickness measurement, each lens produced strong interference fringes, except for extremely large focal lengths (e.g. 200 mm and 400 mm) where the two beams were not large enough to overlap at the location of the camera, leading to weaker or washed-out overlaps. Hence, we report only the results from the 25.4–100 mm range. As seen in Table I, all lenses agree within about ±0.05 mm, except for the 50 mm lens data point, which yields a notably higher thickness (1.37 mm). This discrepancy likely arises from subtle alignment drift, a slightly off-center waist, or possible saturation in the camera image. Nevertheless, the weighted mean $t = (1.028 \pm 0.020)$ mm agrees with the thickness we visually estimated using a ruler, further supporting the validity of the interference-based method.

Sources of Error and Improvements. Several factors may have influenced both measurements. For one, residual s-polarization would artificially shift the Brewster's angle dip. A more stable polarization setup could lower

the reflectance floor near θ_B. Moreover, small tilts in the lens or sample can significantly change the overlap of the two beams for thickness measurements or shift the reflected spot for Brewster's angle. For large focal lengths, the spot may become too large or saturate part of the camera, compromising fringe clarity. Conversely, for very short focal lengths, geometric aberrations or dust on the lens might degrade the pattern. Lastly, the discrete angles (Brewster scan) and the manual fringe center-picking both introduce some user-dependent variability.

Despite these potential pitfalls, our results for both n and t show good agreement with expected values for soda-lime glass. By carefully refining alignment and polarization control, one could reduce the error bars further and achieve a closer match to theoretical wave-optics predictions.

Acknowledgements

These experiments were performed in collaboration with Aleksandar Radak, Cameron Brown, and Bhavya Chugh.

[1] Edmund Optics. "Allied Vision Alvium 1800 U-500M Camera Specifications." Accessed March 25, 2025. https://www.edmundoptics.ca/p/allied-vision-alvium-1800-u-500m-125-50mp-c-mount-\protect\penalty\z@right-angle-usb-31-monochrome-camera/42327

[2] Keysight Technologies, *InfiniiVision 1000 X-Series Oscilloscopes Data Sheet*, Accessed March 27, 2025. https://www.keysight.com/ca/en/assets/7018-06411/data-sheets/5992-3484.pdf, 2019.

[3] NIST, "Refractive Index of Optical Materials," *NIST Electromagnetic Wave Propagation ToolBox*, https://emtoolbox.nist.gov/Wavelength/Documentation.asp, accessed Mar. 28, 2025.

[4] J. Peatross and M. Ware, *Physics of Light and Optics*, 1st ed. (BYU Academic Publishing, 2011). Available at http://optics.byu.edu/BYUOpticsBook.pdf

[5] Processing Foundation, *Processing: A Programming Handbook for Visual Designers and Artists*. https://processing.org/, accessed Mar. 27, 2025.

[6] M. Rubin, "Refractive index of soda-lime glass (Rubin-clear)," *RefractiveIndex.INFO*, https://refractiveindex.info/?shelf=glass&book=soda-lime&page=Rubin-clear, accessed Mar. 28, 2025.

[7] Newport Corporation, "Focusing and Collimating," https://www.newport.com/n/focusing-and-collimating, accessed Mar. 27, 2025.

[8] Wikipedia contributors, "Double-slit experiment," *Wikipedia, The Free Encyclopedia*, https://en.wikipedia.org/wiki/Double-slit_experiment, accessed Mar. 27, 2025.